ACS OMEGA

http://pubs.acs.org/journal/acsodf

Article

Effect of the Deposition Conditions on the Anion Resin Exchange Precipitation of Indium(III) Hydroxide

Natalia Evsevskaya,* Elena Pikurova, Svetlana V. Saikova, and Ivan Vasilievich Nemtsev

Cite This: *ACS Omega* 2020, 5, 4542−4547

Read Online

ACCESS | Metrics & More | Article Recommendations

ABSTRACT: A new patented method for the synthesis of nanosized powders of indium(III) hydroxide and oxide using the strong base anion exchange resin AV-17-8 as a precipitate agent was proposed. The effect of anions of the initial indium salt and the influence of the process duration, temperature, and counterions of resin such as hydroxide or carbonate on the yield of indium(III) hydroxide during the anion resin exchange precipitation were investigated by scanning electron microscopy, electrical conductivity measurement method, and atomic absorption analysis. Based on the obtained data, the mechanism of the anion resin exchange precipitation of indium(III) hydroxide was suggested. The products were characterized by X-ray diffraction, thermogravimetric analysis/differential scanning calorimetry, elemental analysis, Brunauer−Emmett−Teller, and transmission electron microscopy. It was found that impurity-free monophasic In_2O_3 powders with an average particle size of 10−15 nm and specific surface area of 62−73 m^2/g were formed after heat treatment of as-prepared products at 400 °C.

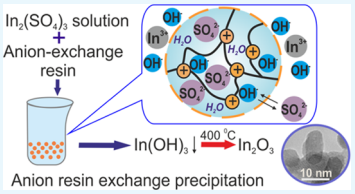

INTRODUCTION

Indium(III) oxide, In_2O_3, is an optically transparent (in the visible range (80−90%)) semiconductor oxide with high electrical conductivity. Thus, In_2O_3 is widely used for the production of numerous optical electronic devices equipped with touch screen, LCD, and plasma TVs, solar cells, and highly sensitive gas sensors.[1−5] In electronics, one of the most popular materials is indium tin oxide (ITO), representing a mixture of In_2O_3 and SnO_2, usually in a mass ratio of 9:1.[6,7]

Generally, the materials based on indium oxide are obtained from the high-reactive precursor $In(OH)_3$ because their characteristics directly affect the properties of the product. Therefore, the development of new synthetic strategies for the production of indium(III) hydroxide with chemical homogeneity, containing particles of similar size and morphology, is a current problem.

The most common methods used to synthesize $In(OH)_3$ are the chemical precipitation from salt solution,[8−12] hydrothermal or solvothermal synthesis,[13−18] sol−gel process,[19,20] and their combinations.[21,22] In the case of the solvothermal (hydrothermal) process, the initial salts of indium or as-precipitated $In(OH)_3$ are kept in an autoclave in aqueous solution or organic solvents at high temperature and pressure, usually, in the presence of surfactants. This approach allows one to obtain products with precisely defined morphology (nanorods, nanocubes, hollow spheres, etc.), and the finest products as compared with other methods. However, the solvothermal method requires the use of complex, expensive equipment, high pressure, being limited by the small size of the reaction chambers. For the sol−gel synthesis, expensive gel-forming components are used, and long synthesis time is required, as well as the control of the hydrolysis rate of the initial reagents to avoid microheterogeneity in the system.

The chemical precipitation method requires the control of the pH value and reaction conditions. Also, as-prepared precipitate particles tend to trap the mother liquor ions; therefore, long-term thorough washing is needed to remove all the adsorbed species, which results in the formation of a large amount of rinsing water subjected to disposal. Each technique presented has some disadvantages; therefore, the creation of new modifications of the known method is an urgent problem.

For the synthesis of precursors of oxide materials, the so-called anion resin exchange precipitation of metal ions is perspective.[23−26] Ion exchange resins are widely used in different separation, purification, and decontamination processes. In the case of anion resin exchange precipitation, a resin or polymer acts as a reagent. This method involves two combined heterogeneous reactions: anion exchange between the sorbent solution and precipitation of an insoluble metal compound from the solution. The process of obtaining $In(OH)_3$ can be described by the equations:

$$InA_3 + 3ROH \rightarrow In(OH)_3 \downarrow + 3RA, \quad (1)$$

Received: November 14, 2019
Accepted: February 14, 2020
Published: February 25, 2020

https://dx.doi.org/10.1021/acsomega.9b03877
ACS Omega 2020, 5, 4542−4547

$$2InA_3 + 3R_2CO_3 + (3 - 2x)H_2O \rightarrow 2In(OH)_{3-2x}(CO_3)_x \downarrow + 6RA + (3 - 2x)CO_2\uparrow \quad (2)$$

R is the anion exchange resin (A = Cl^-, $1/2SO_4^{2-}$, NO_3^-).

This process should be considered as a special case of ion exchange complicated by the precipitation reaction. The method results in nearly complete conversion of reagents and high selectivity, reducing material and energy costs associated with eliminating the necessity of additional purification of products, and, as a result, simplifying the technology design of production, as reported in ref 27.

Herein, we provide patented by us[28] the anion resin exchange precipitation method to obtain $In(OH)_3$ and In_2O_3 nanopowders. As far as we know, the anion resin exchange precipitation method was not used earlier to produce these materials. The influence of various conditions on this process was investigated, and the obtained products were characterized.

RESULTS AND DISCUSSION

Anion Resin Exchange Precipitation of Indium(III) Hydroxide. To control reactions 1 and 2, the specific electrical conductivity of the reaction solutions was measured during the synthesis (Figure 1). The chemical reaction of the anion resin exchange precipitation reduces the number of ions in the solution because the anions of the initial indium salt are absorbed by the resin and the In^{3+} ions are bound into a solid product with ions from the resin: In-OH for the OH form and In-CO_3 for R-CO_3. Uncharged species in the solution do not carry any charge, and then a decrease of the specific electrical conductivity of the reaction solution is observed. As we discussed earlier,[29] in the case of the anion resin exchange precipitation, the charge and diameter of hydrated anions are the main factors affecting the effectiveness of the process. As can be seen in Figure 1a, when $In_2(SO_4)_3$ is used, the SEC of the solution goes down to zero rapidly (30 min), and the formation of a dense white precipitate is observed. In the case of using other indium salts, $In(NO_3)_3$ or $InCl_3$, after 1 h, the SEC reaches about 100 μS/m and remains constant over time. Moreover, the precipitate formation does not occur, but sols are formed, which are transformed into gels with time. In general, the extent of precipitation of indium ions decreases in the row $In_2(SO_4)_3 > InCl_3 \approx In(NO_3)_3$, which is in agreement with the order of affinity for strongly basic anion exchangers.[27] In the subsequent experiments, the anion resin exchange precipitation of indium was carried out only from its sulfate solutions.

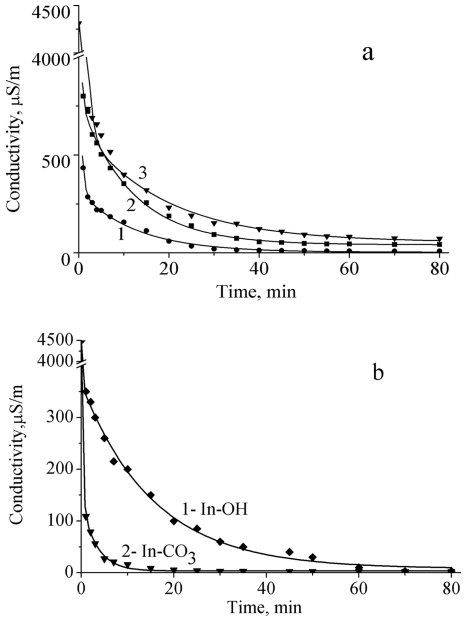

Figure 1. Time dependence of the specific electrical conductivity (SEC) of the reaction solutions during the anion resin exchange precipitation: (a) In-OH from 1: $In_2(SO_4)_3$, 2: $InCl_3$, 3: In $(NO_3)_3$; (b) 1: In-OH; 2: In-CO_3 from $In_2(SO_4)_3$.

Figure 1b shows a change over time for the specific electrical conductivity of the solutions during the anion resin exchange precipitation of indium(III) sulfate in the presence of the resins in OH and CO_3 forms. The SEC of the solution is dramatically decreased to 0 during 10 min by using the resin in the carbonate form, whereas in the case of the OH form, the conductivity at the time is 200 μS/m (Figure 1b). In addition, the molar fraction of In^{3+} (χ) in contact solution during 10 min after the start of the synthesis is also decreased to 2% when the resin in the carbonate form was used (Figure 2, curve 3b),

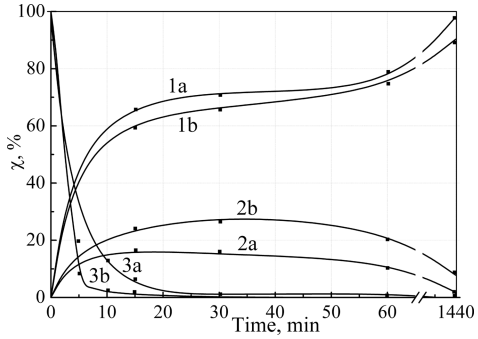

Figure 2. Molar fraction of In^{3+} (χ) in the phases: 1: precipitate, 2: anion exchange resin, 3: contact solution during the anion exchange precipitation of (a) In-OH and (b) In-CO_3.

whereas during the same time, χ decreased to 20% in the presence of the resin in OH form (Figure 2, curve 3a). This result may be explained by a higher pH value of the solution when using the anion exchange resin in the carbonate form (Table 1). This is probably due to a more intensive emission of the acid gas CO_2. However, the indium hydroxide amount when it is an individual phase increases faster if we use the resin in the OH form (Figure 2, curves 1a and 1b). At the same time, a significant amount of indium hydroxide is deposited on

Table 1. Influence of the Reaction Conditions on the Yield of the Product (Deposition Time: 1 h)

		temperature (°C)				
no.	product	initial	final	pH	molar ratio fraction of surface deposit (%)	product yield (%)
1	In-OH	23	23	6	17	68
2		60	60	6	15	75
3		60	15	6	3	95
4	In-CO_3	23	23	7.5	27	62
5		60	60	7.5	17	70
6		60	15	7.5	2	87

https://dx.doi.org/10.1021/acsomega.9b03877
ACS Omega 2020, 5, 4542−4547

the resin bead surface. The indium ions detected in the resin phase (Figure 2, curves 2a and 2b) are caused by the dissolution of surface deposit $In(OH)_3$ during the acid treatment of the resin. It is noticeable that the sorption of indium cations by the strong base anion exchanger resin is excluded due to the positive Donnan potential at the interface.

Then, during further precipitation, the product yield (Figure 2, curves 1a and 1b) increased up to 96 and 88% during 24 h for OH and CO_3 forms of the resin, respectively. At the same time, the amount of indium in the resin phase decreased.

According to electron microscopy (Figure 3), after 15 min of the synthesis, the surface of the resin beads was almost

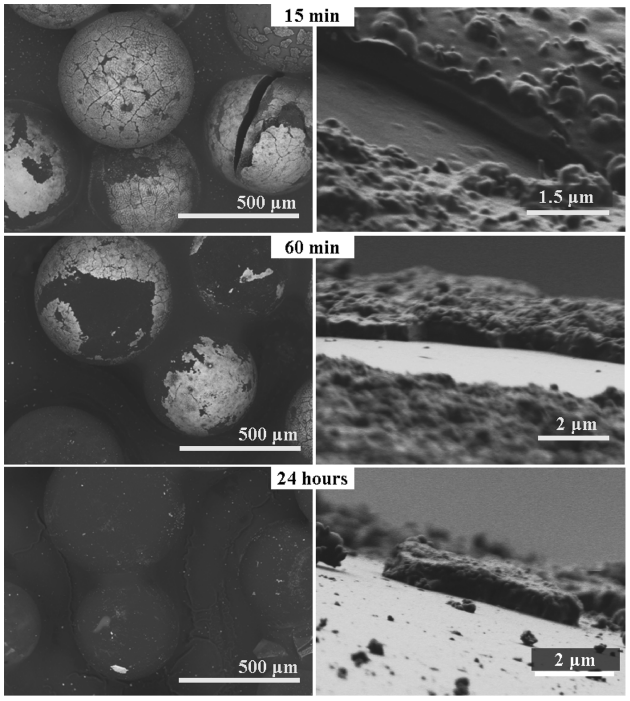

Figure 3. SEM micrographs of the grain surface of the anion resin AV-17-8 (CO_3) during the synthesis of In-CO_3.

completely covered by a layer of a surface deposit. These data are given for the carbonate form of resin, and the results obtained for OH form are similar. The surface deposit started to flake away from the resin beads after 30−60 min since the areas of the cleared bead surfaces could be seen. The deposit is assumed to have been exfoliated when reaching a thickness of about 1 μm. The SEM data revealed that the complete desorption occurred within 24 h.

Thus, we can suggest the following mechanism of the anion resin exchange precipitation of indium(III) hydroxide: the anion exchange between the anions of indium solution and the resin, the formation of indium hydroxide on the surface of the resin beads, exfoliation of the deposit layer after increasing the thickness to 1 μm and more, and deposition onto the vessel bottom as an individual product phase. Moreover, these processes occur almost simultaneously.

As can be seen in Figure 3, the deposit layer has cracks through which the diffusion might occur. Therefore, the precipitate on the surface of the grain does not block ion exchange but reduces the rate, and the process continues until a complete conversion of the reagents occurs. The rate-limiting stage of the overall process is the surface deposit desorption. It is assumed that in the case of the resin in CO_3 form, a closer deposit with higher adhesive properties is formed; therefore, more time is needed for it to flake away than in the case of using the anion exchanger in hydroxide form.

To increase the desorption rate and decrease the adsorbed metal amount, the process was carried out at 60 °C. The effect of increasing temperature produced a positive impact on the product yield (Table 1, samples 2 and 5). However, the amount of the adsorbed deposit remained significant, 15 and 17% for OH and CO_3 forms, respectively. In the subsequent experiments, we used the temperature gradient: after the reaction proceeding for 1 h at 60 °C, the mixture was rapidly cooled to 15 °C in an ice bath. This procedure led to the rapid exfoliation of the surface deposit due to the difference in coefficients of thermal expansion of the surface deposit and resin. The indium content in the resin phase decreased to 2−3%, and the product yield increased up to 95 and 87% (Table 1, samples 3 and 6).

The optimum reaction conditions providing up to 95% yield of indium hydroxide were as follows: the strong base anion exchange resin in OH or CO_3 form, with the concentration of $In_2(SO_4)_3$ solution being 0.25 M, processing time being 1 h at a temperature of 60 °C, followed by cooling to 15 °C in the ice bath.

Characterization of the Products. The composition of as-precipitated products obtained under the optimum reaction conditions using the anion resin in CO_3 form (named In-CO_3) and OH form (named In-OH) was determined by elemental (atomic absorption spectroscopy, EDX, CHNS/O analysis) and complex thermal analysis. It is represented by the following formulas: $In(OH)_{2.64}(CO_3)_{0.18}$ for the In-OH sample and $In(OH)_{1.94}(CO_3)_{0.53}$ for the In-CO_3 sample. The presence of carbonate ions in the In-OH sample can be explained by the CO_2 adsorption from air by both the anion resin[29] and the precipitate during the drying procedure in the oven. In addition, hydroxide ions were detected in the In-CO_3 sample due to the hydrolysis of indium carbonate.

Figure 4 shows the thermal behavior of the In-CO_3 sample. The mass loss that occurred up to 150 °C and an endothermic

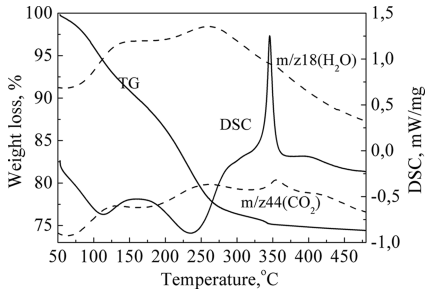

Figure 4. TG, DSC, and mass spectrum of the released gases during heating (H_2O, CO_2) for In-CO_3.

peak at 115 °C on the DSC curve were mainly due to the removal of surface-adsorbed water molecules. Another significant mass loss was noted in a range from 200 °C to 300 °C. The following endothermic effect has maximum at 236 °C. It corresponds to the release of carbon dioxide and water due to the thermal conversion of indium hydroxide carbonate to In_2O_3. An exothermal sharp peak at 346 °C is likely to be attributed to the crystallization of the final product. The thermal behavior of the In-OH sample is similar, but carbon

https://dx.doi.org/10.1021/acsomega.9b03877
ACS Omega 2020, 5, 4542−4547

dioxide release is slightly lower. According to energy-dispersive X-ray spectroscopy (Figure 5a,b), the composition of the

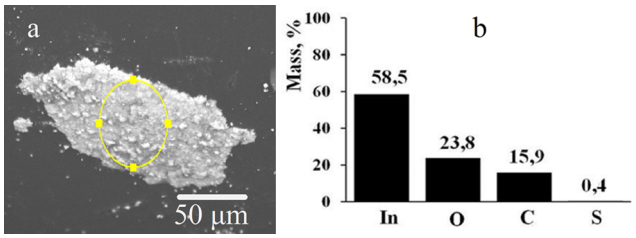

Figure 5. SEM micrograph of the surface deposit on the AV-17-8(CO_3) resin bead during the synthesis of In-CO_3, with (a) the marked area for X-ray microanalysis and (b) mass fractions of the elements in this area.

surface deposit corresponds to the crystals deposited on the vessel bottom. Sulfate is not detected in the product. Since the analysis depth is up to 1.5 μm, which is more than the surface deposit thickness, a small amount of sulfur (0.4%) determined by X-ray spectroscopy could be attributed to sulfate ions, which have been sorbed by the resin during the process.

Figure 6 shows the diffraction patterns of the In-CO_3 and In-OH as-prepared samples and of the samples after calcination at

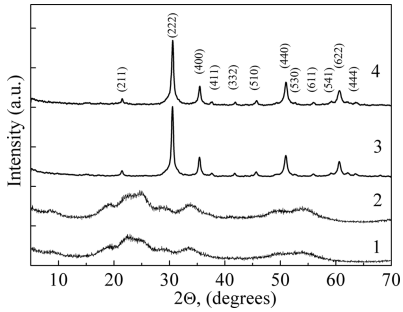

Figure 6. X-Ray diffraction patterns of the In-OH (1), In-CO_3 (2), In-OH-400 (3), In-CO_3−400 (4).

400 °C. As can be seen from curves 1 and 2, there are no clearly defined peaks, that is, these samples are amorphous and cannot be associated with any known In$(OH)_3$ or InOOH peaks. These samples may be related to an amorphous intermediate compound generated by anion exchange precipitation. After calcination of In-CO_3 and In-OH precursors at 400 °C (samples In-OH-400 and In-CO_3−400), the diffraction peaks in both cases (curves 3 and 4) agreed well with that of a body-centered cubic phase In_2O_3 (JCPDS file no. 74-1990). No peaks evidencing other crystal phases have been detected. The crystallite size, calculated using the Debye−Scherrer equation for the four most intensive peaks, was 15.8 nm for the In-OH-400 sample and 14.3 nm for the In-CO_3−400 sample. According to the TEM data (Figure 7), the particle size of the In-CO_3 sample was approximately 8−10 nm and of the In-OH sample was 10−12 nm, which is close to the XRD data. In addition, the specific surface area was measured using the BET model, being 73 and 62 m^2/g for In-CO_3 and In-OH, respectively. Based on these data, the particle sizes were calculated using the equation given in ref 31 amounting to 13 and 11 nm. The obtained values of the particle size were in good agreement with the TEM data and with the calculated sizes from the XRD data. These

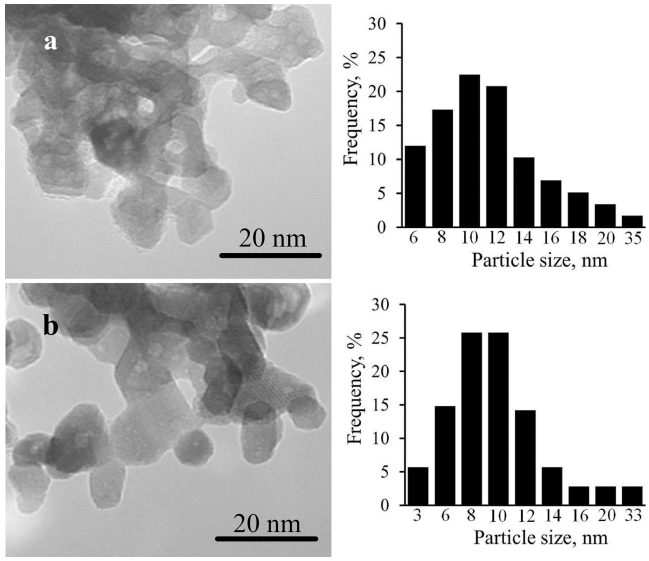

Figure 7. TEM micrographs and histograms of the particle size distribution of the In_2O_3, samples obtained for (a) In-CO_3 and (b) In-OH.

characteristics are similar to the results obtained by Latha et al.[32] by the thermal decomposition at 650 °C of indium(III) acetylacetonate with acacia gum and surfactants cetyl trimethyl ammonium bromide (CTAB) and sodium docecyl benzene sulfonate (SDBS), but we do not use expensive and toxic reagents. Lee et al.[9] have obtained indium oxide with a particle size of 10−15 nm by the chemical deposition method. However, in our case, the control of the synthesis conditions is easier, since it proceeds under stationary conditions at a constant pH value and the precipitation product is not contaminated with ions of the mother liquor.

Thus, the types of the resin counterions (OH^- or CO_3^{2-}) had no significant effect on the particle size of the produced indium oxide. The samples obtained using the resin consist of nanoscale particles, have a large specific surface area, and show high reaction activity. It is could be explained by additional gas (carbon dioxide) emission during the synthesis (reaction 2) and further heat treatment of the product (Figure 4) that produces more porous structures.

CONCLUSIONS

In the present study, the process of anion resin exchange precipitation of indium(III) hydroxide by using the electrical conductivity measurement method, SEM, X-ray microanalysis, and chemical analysis was thoroughly studied. Based on the obtained data, the mechanism of the process, proceeding through the stages of anion exchange between the anions of indium solution and the resin, the precipitation of indium hydroxide on the surface of the resin beads, and the rate-limiting stage of the surface deposit desorption with the formation of an individual product phase, was proposed.

The optimum reaction conditions providing the maximum product yield were as follows: the strong base anion exchange resin in OH or CO_3 form, with the concentration of $In_2(SO_4)_3$ solution being 0.25 M, processing time being 1 h at a temperature of 60 °C, followed by cooling to 15 °C in the ice bath. According to TG-DSC and elemental analysis, in the presence of the AV-17-8(OH) resin, the product with the molecular formula In$(OH)_{2.64}(CO_3)_{0.18}$ was obtained, while in

https://dx.doi.org/10.1021/acsomega.9b03877
ACS Omega 2020, 5, 4542−4547

the case of AV-17-8(CO_3), the obtained product was $In(OH)_{1.94}(CO_3)_{0.53}$.

In addition, the as-prepared deposits after the heat treatment at 400 °C were transformed to impurity-free monophase In_2O_3 powders with an average particle size of 10−15 nm and specific surface area of 62−73 $m^2\ g^{-1}$. The obtained materials are promising as precursors for the preparation of indium tin oxide; they can also be used in modern electronics.

MATERIALS AND METHODS

Indium nitrate $In(NO_3)_3{\cdot}4{\cdot}5H_2O$, indium chloride $InCl_3{\cdot}3H_2O$, and indium sulfate $In_2(SO_4)_3{\cdot}xH_2O$ were purchased from Sigma-Aldrich. The strong base anion exchange resin AB-17-8 with a polystyrenic gel matrix was produced by "Azot" Corporation (Cherkassy, Ukraine) in the chloride form with a bead size of 0.4−0.6 mm (Russian GOST 20301-74). This resin has a gel matrix based on polystyrene cross-linked with divinylbenzene and functional group quaternary ammonium (type I). This resin is an analogue of Purolite A400/A300, Lewatit M-500, Amberlite IRA 402/420, Dowex SBR-P/Maraton A, has a significantly lower cost and is widely used in different separation, purification, and decontamination processes in Russia. Preliminary tests[23,24,33] of AV-17-8 showed trends similar to A400/A300 resin. The conversion of resin to the hydroxyl or carbonate form and the determination of its total exchange capacity, that is, the total number of sites available for exchange, were carried out according to the techniques described in our works.[24,30] The total exchange capacity of the anion exchange resin in the hydroxide form was 1.0 meq·g^{-1} and that in the carbonate form was 0.7 meq·ml^{-1}.

In typical experiments, AV-17-8(CO_3) or (OH) taken in excess (150%) is added to 0.25 M solution of indium salt. The mixture was stirred (200 rpm) at a temperature of 20−60 °C using a magnetic stirrer for a specified time: from 15 min to 24 h. To remove the anion exchange resin beads from the reaction products, a sieve with round holes 0.1 mm in diameter was used and the precipitate was centrifuged, washed with distilled water, and finally dried in air at 80 °C to form a precursor. The resin was also washed with distilled water and eluted three times with 1 M HNO_3 (10 mL portions) while stirring for 1 h. All the aqueous samples (eluates, stock solutions, dissolved precipitates) were analyzed for indium using a PerkinElmer A Analyst 400 Atomic-Absorption spectrometer (USA). The molar fraction of In^{3+} (χ, %) in each phase was calculated using the formula

$$\chi = n^{eq}/n^0 \cdot 100\%,$$

where n^{eq} is the number of moles of In^{3+} in the phase (precipitate, anion exchange resin, stock solution) and n^0 is the number of moles In^{3+} in the solution at the initial moment of time.

The specific electrical conductivity (SEC) of the reaction solutions was measured using a Multitest KSL-101 (Semikocompany, Novosibirsk, Russia).

In_2O_3 samples were obtained by heat treatment of the precursors in a muffle furnace for 1 h at 400 °C.

The surface of the anion exchange resin beads during the precipitation was investigated by SEM. Small portions of resin (less than 1% of the total amount) were removed from the reaction vessel after a certain time interval (15, 30, and 60 min and 24 h), washed with distilled water, dried at 60 °C, and fixed on an aluminum plate 5 × 7 × 0.3 mm using epoxy resin. Micrographs and elemental mapping of the resin beads surface were performed using a TM-3000 desktop scanning electron microscope (Hitachi, Japan) equipped with a BRUKER XFlash 430 H X-ray analyzer.

The thermochemical analysis of the precursors was conducted by thermogravimetry and differential scanning calorimetry (TG-DSC, NETZSCH STA449C) in a temperature range of 25−900 °C at a heating rate of 10 °C min^{-1} in flowing air (30 mL min^{-1}). The analysis of evolved gases during the sample heating was carried out using a quadrupole mass spectrometer QMS 403 C Aëolos (NETZSCH).

Powder X-ray diffraction was carried out using a Shimadzu XRD-7000S diffractometer equipped with a Cu Kα anode. The carbon content in the samples was determined using the Flash EA 1112 instrument from Thermo Fisher Scientific. Nitrogen adsorption was measured using an ASAP 2420 instrument (Micromeritics) at T = 77.3 K. The specific surface area was calculated using the BET model. The degassing of the samples was carried out in two stages: at 150 for 3 h and at 250 °C for 3 h under 0.5 to 800 mmHg pressure in a degassing port. Transmission electron microscopy (TEM) was carried out using a HT-7700 instrument (Hitachi, Japan) operating at an accelerating voltage of 100 kV.

AUTHOR INFORMATION

Corresponding Author

Natalia Evsevskaya − *Institute of Chemistry and Chemical Technology SB RAS, Federal Research Center "Krasnoyarsk Science Center SB RAS", Krasnoyarsk 660036, Russia;* orcid.org/0000-0001-5020-9943; Email: yevsevskaya@gmail.com

Authors

Elena Pikurova − *Institute of Chemistry and Chemical Technology SB RAS, Federal Research Center "Krasnoyarsk Science Center SB RAS", Krasnoyarsk 660036, Russia*

Svetlana V. Saikova − *Institute of Chemistry and Chemical Technology SB RAS, Federal Research Center "Krasnoyarsk Science Center SB RAS", Krasnoyarsk 660036, Russia; Siberian Federal University, Krasnoyarsk 660041, Russia*

Ivan Vasilievich Nemtsev − *Federal Research Center "Krasnoyarsk Science Center SB RAS", Krasnoyarsk 660036, Russia; Kirensky Institute of Physics, Federal Research Center "Krasnoyarsk Science Center SB RAS", Krasnoyarsk 660036, Russia*

Complete contact information is available at: https://pubs.acs.org/10.1021/acsomega.9b03877

Notes

The authors declare no competing financial interest.

ACKNOWLEDGMENTS

The work was supported by the Russian Foundation for Basic Research (RFBR): grant no. 18-33-00504. The authors thank the Federal Research Center "Krasnoyarsk Science Center of the Siberian Branch of the Russian Academy of Sciences" for using its facilities.

REFERENCES

(1) Lu, J. G.; Chang, P.; Fan, Z. Quasi-one-dimensional metal oxide materials—Synthesis, properties and applications. *Mater. Sci. Eng., R* **2006**, *52*, 49−91.

https://dx.doi.org/10.1021/acsomega.9b03877
ACS Omega 2020, 5, 4542−4547

(2) Exarhos, G. J.; Zhou, X. D. Discovery-based design of transparent conducting oxide films. *Thin Solid Films* **2007**, *515*, 7025−7052.
(3) Freeman, A. J.; Poeppelmeier, K. R.; Mason, T. O.; Chang, R. P. H.; Marks, T. J. Chemical and Thin-Film Strategies for New Transparent Conducting Oxides. *MRS Bull.* **2000**, *25*, 45−51.
(4) Mahalingam, S.; Abdullah, H. Electron transport study of indium oxide as photoanode in DSSCs: A review. *Renewable Sustainable Energy Rev.* **2016**, *63*, 245−255.
(5) Granqvist, C. G. Transparent conductors as solar energy materials: A panoramic review. *Sol. Energy Mater. Sol. Cells* **2007**, *91*, 1529−1598.
(6) Rembeza, S.; Voronov, P.; Rembeza, E. Synthesis and Physical Properties of Nanocomposites $(SnO_2)_x(In_2O_3)_{1-x}$ (x=0−1) for Gas Sensors and Optoelectronics. *Sens. Transducers J.* **2010**, *122*, 46−54.
(7) Gilstrap, R. A., Jr.; Capozzi, C. J.; Carson, C. G.; Gerhardt, R. A.; Summers, C. J. Synthesis of a Nonagglomerated Indium Tin Oxide Nanoparticle Dispersion. *Adv. Mater.* **2008**, *20*, 4163−4166.
(8) Li, C.; Lian, S.; Liu, Y.; Liu, S.; Kang, Z. Preparation and photoluminescence study of mesoporous indium hydroxide nanorods. *Mater. Res. Bull.* **2010**, *45*, 109−112.
(9) Lee, W. J.; Choi, E. K.; Han, K. S.; Kim, J. H.; Kim, U. S.; Hwang, K. T.; Shim, K. B.; Hwang, H. J.; Cho, W. S. Structural evolution of indium hydroxide powders prepared by a precipitation method. *J. Ceram. Process. Res.* **2018**, *19*, 272−278.
(10) Frei, M. S.; Capdevila-Cortada, M.; García-Muelas, R.; Mondelli, C.; López, N.; Stewart, J. A.; Curulla Ferré, D.; Pérez-Ramírez, J. Mechanism and microkinetics of methanol synthesis via CO_2 hydrogenation on indium oxide. *J. Catal.* **2018**, *361*, 313−321.
(11) Tao, X.; Sun, L.; Li, Z.; Zhao, Y. Side-by-Side $In(OH)_3$ and In_2O_3 Nanotubes: Synthesis and Optical Properties. *Nanoscale Res. Lett.* **2010**, *5*, 383−388.
(12) Goh, K. W.; Johan, M. R.; Wong, Y. H. Enhanced structural properties of In_2O_3 nanoparticles at lower calcination temperature synthesised by co-precipitation method. *Micro Nano Lett.* **2017**, *13*, 270−275.
(13) Zhu, H.; Wang, Y.; Wang, N.; Li, Y.; Yang, J. Hydrothermal synthesis of indium hydroxide nanocubes. *Mater. Lett.* **2004**, *58*, 2631−2634.
(14) Zhuang, Z.; Peng, Q.; Liu, J.; Wang, X.; Li, Y. Indium hydroxides, oxyhydroxides, and oxides nanocrystals series. *Inorg. Chem.* **2007**, *46*, 5179−5187.
(15) Lin, L.-T.; Tang, L.; Zhang, R.; Deng, C.; Chen, D.-J.; Cao, L.-W.; Meng, J.-X. Monodisperse In_2O_3 nanoparticles synthesized by a novel solvothermal method with $In(OH)_3$ as precursors. *Mater. Res. Bull.* **2015**, *64*, 139−145.
(16) Li, B.; Xie, Y.; Jing, M.; Rong, G.; Tang, Y.; Zhang, G. In_2O_3 hollow microspheres: Synthesis from designed $In(OH)_3$ precursors and applications in gas sensors and photocatalysis. *Langmuir* **2006**, *22*, 9380−9385.
(17) Du, J.; Yang, M.; Cha, S. N.; Rhen, D.; Kang, M.; Kang, D. J. Indium Hydroxide and Indium Oxide Nanospheres, Nanoflowers, Microcubes, and Nanorods: Synthesis and Optical Properties. *Cryst. Growth Des.* **2008**, *8*, 2312−2317.
(18) Yu, N.; Dong, D.; Qi, Y.; Gui, J. Growth of Indium Hydroxide Nanocubes Film by Hydrothermal Method. *J. Nanosci. Nanotechnol.* **2017**, *17*, 1476−1479.
(19) Ramanathan, G.; Xavier, R. J.; Murali, K. R. Sol Gel Dip Coated Indium Oxide Films and Their Properties. *ECS Trans.* **2012**, *41*, 33−38.
(20) Forsh, E. A.; Abakumov, A. M.; Zaytsev, V. B.; Konstantinova, E. A.; Forsh, P. A.; Rumyantseva, M. N.; Gaskov, A. M.; Kashkarov, P. K. Optical and photoelectrical properties of nanocrystalline indium oxide with small grains. *Thin Solid Films* **2015**, *595*, 25−31.
(21) Gurlo, A.; Dzivenko, D.; Andrade, M.; Riedel, R.; Lauterbach, S.; Kleebe, H. J. Pressure-Induced Decomposition of Indium Hydroxide. *J. Am. Chem. Soc.* **2010**, *132*, 12674−12678.
(22) Askarinejad, A.; Iranpour, M.; Bahramifar, N.; Morsali, A. Synthesis and characterisation of $In(OH)_3$ and In_2O_3 nanoparticles by sol-gel and solvothermal methods. *J. Exp. Nanosci.* **2010**, *5*, 294−301.
(23) Pashkov, G. L.; Saikova, S. V.; Panteleeva, M. V.; Linok, E. V.; Evsevskaya, N. P.; Bondarenko, G. N.; Zhizhaev, A. M.; Tarasova, L. S. Anion-Exchange Synthesis of Yttrium-Aluminum Garnet Powders. *Glass Ceram.* **2016**, *73*, 107−110.
(24) Ivantsov, R.; Evsevskaya, N.; Saikova, S.; Linok, E.; Yurkin, G.; Edelman, I. Synthesis and characterization of $Dy_3Fe_5O_{12}$ nanoparticles fabricated with the anion resin exchange precipitation method. *Mater. Sci. Eng. B* **2017**, *226*, 171−176.
(25) Taglieri, G.; Daniele, V.; Macera, L. Synthesizing Alkaline Earth Metal Hydroxides Nanoparticles through an Innovative, Single-Step and Eco-Friendly Method. *Solid State Phenom.* **2019**, *286*, 3−14.
(26) Kobayashi, Y.; Morimoto, H.; Nakagawa, T.; Kubota, Y.; Gonda, K.; Ohuchi, N. Fabrication of gadolinium hydroxide nanoparticles using ion-exchange resin and their MRI property. *J. Asian Ceram. Soc.* **2016**, *4*, 138−142.
(27) Pashkov, G. L.; Saikova, S. V.; Panteleeva, M. V. Reactive ion exchange processes of nonferrous metal leaching and dispersion material synthesis. *Theor. Found. Chem. Eng.* **2016**, *50*, 575−581.
(28) Pashkov, G. L.; Saikova, S. V.; Panteleeva, M. V.; Evsevskaya, N. P. RF Patent no. US 2,587,083 A, Byull. Izobret. No. 16, 2016.
(29) Pashkov, G. L.; Saikova, S. V.; Panteleeva, M. V.; Linok, E. V. Ion-exchange synthesis of α-modification of nickel hydroxide. *Theor. Found. Chem. Eng.* **2014**, *48*, 671−676.
(30) Saikova, S. V.; Panteleeva, M. V.; Nikolaeva, R. B.; Pashkov, G. L. Optimal Conditions of Ion-Exchange Synthesis of Cobalt (II) Hydroxide with AV-17-8 Anion Exchanger in the OH Form. *Russ. J. Appl. Chem.* **2002**, *75*, 1787−1790.
(31) Ayeshamariam, A.; Kashif, M.; Muthu Raja, S.; Sivaranjani, S.; Sanjeeviraja, C.; Bououdina, M. Synthesis and characterization of In_2O_3 nanoparticles. *J. Korean Phys. Soc.* **2014**, *64*, 254−262.
(32) Latha, C. K.; Raghasudha, M.; Aparna, Y.; Ramchander, M.; Ravinder, D.; Jaipal, K.; Veerasomaiah, P.; Shridhar, D. Effect of Capping Agent on the Morphology, Size and Optical Properties of In_2O_3 Nanoparticles. *Mater. Res.* **2017**, *20*, 256−263.
(33) Saikova, S. V.; Kirshneva, E. A.; Panteleeva, M. V.; Pikurova, E. V.; Evsevskaya, N. P. Production of Gadolinium Iron Garnet by Anion Resin Exchange Precipitation. *Russ. J. Inorg. Chem.* **2019**, *64*, 1191−1198.

https://dx.doi.org/10.1021/acsomega.9b03877
ACS Omega 2020, 5, 4542−4547